

Article

Effect of Ultrasonic Vibration on Microstructure and Antifouling Capability of Cu-Modified TiO₂ Coating Produced by Micro-Arc Oxidation

Pengfei Hu ^{1,†}, Liyang Zhu ^{1,2,†}, Jiejun Liu ³, You Lv ², Guangyi Cai ^{1,*}  and Xinxin Zhang ^{2,*}

¹ National Key Laboratory of Electromagnetic Energy, Naval University of Engineering, Wuhan 430033, China; huhongyi-fei@163.com (P.H.); zly17854173007@163.com (L.Z.)

² Key Laboratory of Material Chemistry for Energy Conversion and Storage, Hubei Key Laboratory of Material Chemistry and Service Failure, School of Chemistry and Chemical Engineering, Huazhong University of Science and Technology, Ministry of Education, 1037 Luoyu Road, Hongshan District, Wuhan 430074, China; lvyou0819@163.com

³ Xiangtan Electric Power Co., Ltd., Xiangtan 411101, China; jiejunliu150@163.com

* Correspondence: cgy54@sina.cn (G.C.); xinxinzhang@hust.edu.cn (X.Z.)

† These authors contribute equally to this work.

Abstract: Ti and its alloys have received wide attention in marine engineering. However, the limited anti-biofouling capability may hinder their wide application. In the present work, micro-arc oxidation (MAO) with and without the introduction of ultrasonic vibration (UV) has been conducted on metallic Ti substrate in an aqueous solution containing Na₂Cu-EDTA to produce a Cu-modified TiO₂ coating. Microstructural characterization reveals that the introduction of UV increased the thickness of the coating (ranging from ~13.5 μm to ~26.2 μm) compared to the coating (ranging from ~8.1 μm to ~12.8 μm) without UV. A relatively higher Cu content (~2.13 wt.%) of the coating with UV relative to the coating (~1.39 wt.%) without UV indicates that UV enhances the incorporation of Cu into TiO₂. Further, both electrochemical properties and the response to sulfate-reducing bacteria (SRB) were evaluated, revealing that UV introduction endows Cu-modified TiO₂ coating with enhanced corrosion resistance and antifouling capability. The present results suggest that ultrasound-auxiliary micro-arc oxidation (UMAO) obviously enhances the surface performance of Ti alloys for promising applications in marine engineering.

Keywords: micro-arc oxidation; ultrasound; Cu-modified TiO₂; corrosion resistance; antifouling



Citation: Hu, P.; Zhu, L.; Liu, J.; Lv, Y.; Cai, G.; Zhang, X. Effect of Ultrasonic Vibration on Microstructure and Antifouling Capability of Cu-Modified TiO₂ Coating Produced by Micro-Arc Oxidation. *Coatings* **2024**, *14*, 376. <https://doi.org/10.3390/coatings14040376>

Academic Editor: Agnieszka Kurc-Lisiecka

Received: 29 February 2024

Revised: 18 March 2024

Accepted: 21 March 2024

Published: 22 March 2024



Copyright: © 2024 by the authors. Licensee MDPI, Basel, Switzerland. This article is an open access article distributed under the terms and conditions of the Creative Commons Attribution (CC BY) license (<https://creativecommons.org/licenses/by/4.0/>).

Highlights

What are the main findings?

- The introduction of ultrasonic vibration promotes Cu incorporation into TiO₂.
- Enhanced corrosion resistance is achieved by introducing ultrasonic vibration.
- The formation of bio-film is effectively hindered on Cu-modified TiO₂ coating.

What is the implication of the main finding?

- Ultrasound-auxiliary micro-arc oxidation (UMAO) obviously enhances the surface performance of Ti alloys for promising applications in marine engineering.
- UV introduction endows Cu-modified TiO₂ coating with enhanced corrosion resistance and antifouling capability, which provides theoretical guidance for surface modification techniques in marine engineering

1. Introduction

Titanium (Ti) and its alloys with excellent corrosion resistance, high specific strength, and high fatigue tolerance are promising material candidates for marine engineering after

years of technical investigations [1]. Nowadays, Ti and its alloys have already been used as seawater cooling pipelines in power plants [2], heat exchangers in desalination plants [3], and fasteners in the marine industry [4], and is also considered to be the next-generation material for ship hulls and subsea equipment [5].

However, even with excellent corrosion resistance, Ti-based components may fail in harsh marine environments [6], which is mainly associated with bio-fouling due to their excellent biocompatibility and the consequent limited antifouling performance [7,8]. Nowadays, it is agreed that the application of Ti in harsh marine environments requires simultaneous improvements in anti-corrosion properties, wear resistance, and antifouling capability [6,9–12].

Since all the above-mentioned processes occur at the material–environment interface, the surface modification technique is thus regarded as an effective method to endow Ti with enhanced resistance to corrosion, wear, and biofouling associated with micro-organisms [10,13]. Nowadays, numerous surface modification methods have been applied [14–16]. Physical vapor deposition (PVD), chemical vapor deposition (CVD), electrophoretic deposition, the sol–gel method, plasma spraying, and hot-dip coating are the main methods of preparing anti-corrosion coatings [17,18]. However, these methods have certain drawbacks, such as the relatively low coating rate of PVD and CVD, the high temperature of the preparation process of plasma spraying, and the sol–gel method may affect the mechanical properties of the substrate [19–21]. Among all present methods, micro-arc oxidation (MAO) is considered to be one of the most promising methods devoid of the listed disadvantages [7,22,23] and involves complex physical and chemical processes at a relatively high applied voltage [24–26]. The effective method for forming micro-arc oxidation coatings is plasma electrolytic oxidation (PEO) in aqueous electrolytes [27] and molten salt [20].

The ceramic coating produced by MAO exhibits high chemical inertness, which thus acts as a physical barrier to improve the corrosion resistance of the Ti substrate [28]. Meanwhile, the high hardness of the ceramic coating also endows the Ti substrate with high wear resistance [29]. Unfortunately, the ceramic coating generally exhibits a limited antifouling capability to prevent the side effects associated with micro-organisms [11], which widely exist in the ocean [9]. After being exposed to seawater, micro-organisms may adhere to the surface and grow to form colonies, which then could form a bio-film and thus result in microbiologically induced corrosion (MIC) [30,31], which may cause the failure of Ti-based components and, consequently, compromise the safe operation of the facilities in marine engineering [10]. Thus, it is necessary to endow TiO₂-based coating with the desirable antifouling capability to ensure the reliability of Ti alloys in the marine industry.

Cu, as an effective antimicrobial agent [32–35], is able to offer desirable antimicrobial capacity by impeding bacteria growth and thus preventing bio-film formation [11]. After the banning of Sn-containing antifouling paints in 2008, copper compounds were increasingly used, which have been proven to be effective during the past decade [36].

The incorporation of Cu species into MAO coatings generally involves two different methods based on Cu sources [33,34,37], which could be either alloyed with the substrate or directly added into the electrolyte. Ti-Cu alloys have been developed as antibacterial bio-medical materials for human implants [33,38]. After micro-arc oxidation, a TiO₂ coating with the presence of CuO could be fabricated, which exhibits desirable antibacterial capability against *S. aureus* bacteria [33]. Similarly, the micro-arc oxidation of Cu-Ti deposited film facilitates the formation of a Cu-modified TiO₂ layer [39], which contains CuO as the dominant antibacterial agent [40]. By contrast, Cu(CH₃COO)₂ [41], Cu(NO₃)₂ [42], and Cu nanoparticles (NPs) [43] have also been applied as electrolytic components to provide the Cu source for the production of the Cu-modified TiO₂ ceramic layer. In recent work, Na₂Cu-EDTA has been proposed as a novel Cu source [34]. Unlike the traditional Cu-containing components, the Cu-EDTA complex, as a negatively charged component, could easily be migrated to the anode, which is conducive to its subsequent incorporation.

However, even with the application of a negatively charged Cu-EDTA complex, the efficacy of Cu incorporation into TiO₂ still remains low [44], which may be disadvantageous for its antifouling capability. To enhance the dosage of incorporated Cu, several new assistance technologies were applied during the MAO process. Among all available assistance technologies, ultrasonic vibration (UV) has been widely applied in numerous fields [25,45–48]. Hence, it is envisioned that the introduction of UV in the MAO process may promote Cu incorporation into TiO₂, which thus ensures the safe operation of Ti-based components in the marine industry.

In this work, UV is introduced into the micro-arc oxidation process, and the influence of UV on the microstructure, corrosion resistance, and antifouling properties of Cu-modified TiO₂ coating has been examined in detail. With the introduction of UV, an increased content of Cu could be incorporated into TiO₂. UV introduction endows Cu-modified TiO₂ coating with enhanced corrosion resistance and antifouling capability, which provides theoretical guidance for surface modification techniques in marine engineering.

2. Experimental Methods

2.1. Preparation of Specimens

Commercial pure titanium (cp-Ti) samples with diameters of 15 mm were cut from a rod in the present work. All samples were mechanically polished to 1200 grit and were subsequently washed in high-purity water and then dried in air.

UMAO was conducted on cp-Ti samples using an in-house setup [44]. The galvanostatic mode was used during the MAO process to fix the current density at 100 mA/cm² through the power supply (YS9000DD, Yisheng, Shenzhen, China). The ultrasonic frequency and power are optimized at 60 kHz and 100 W. The electrolyte consisting of 15.8 g/L calcium acetate, 7.2 g/L sodium dihydrogen phosphate (Sinopharm, Shanghai, China) as well as 5 g/L Na₂Cu-EDTA (XFJ11 and XFJ44, XFNANO, Nanjing, China) was used. For comparison, the conventional MAO without the introduction of ultrasonic vibration was also conducted under the same condition. According to the preparation method, the resulting coatings are referred to as TC-stir and TC-ultra, corresponding to conventional and ultrasound-auxiliary MAO methods, respectively.

2.2. Microstructural and Property Characterization

The phase component of MAO specimens was detected by TF-XRD (thin film X-ray diffraction, XtaLAB PRO MM007HF, Rigaku, Tokyo, Japan). The specific measurement parameters of the experiment were: Cu target Ka radiation, tube voltage 40 kV, tube current 40 mA, scanning range 20°–80°, scanning speed 1° min^{−1} with an incident angle of 0.8°. The surface and cross-sectional morphologies of TC-stir and TC-ultra were observed using a field emission scanning electron microscope (SEM, FEI Nova 450, FEI, Hillsboro, OR, USA) with the application of electron probe X-ray micro-analyzer (EPMA, Shimadzu 8050G, Rigaku, Tokyo, Japan) to detect the elemental compositions. The electron type of the SEM images used to obtain the surface and cross-section of the coatings was secondary electrons, and the SEM images for EPMA analysis are backscattered electron images. The accelerating voltage to generate the EPMA is 15 kV.

For the preparation of cross-sections of samples, the MAO samples were first encapsulated using epoxy resin. The specimens were then sanded step by step using 180#, 800#, and 2000# SiC sandpaper, grinding the specimens sequentially to 4000 mesh silicon carbide sandpaper and polishing them sequentially using 3 μm and 1 μm aluminum oxide polishing solutions. Finally, the specimens were ultrasonically cleaned in ethanol for 10 min and dried in cold air. In order to prevent the specimen from being contaminated, the prepared specimen is vacuum-encapsulated before testing.

Water contact angles (CAs) were measured using an optical contact angle meter (JC2000D, Powereach, Shanghai, China) by dropping 4 μL of de-ionized water droplet onto the specimen surface. The average CA value was obtained from three randomly selected positions.

To characterize the antifouling property of the specimens, sulfate-reducing bacteria (SRB), as a representative micro-organism existing in seawater, has been used in the work. The SRB seed that was identified as *Desulfovibrio* was isolated from the South China Sea (Zhanjiang, Guangdong). Simulated seawater containing nutrients was used for bacterial culture and corrosion test medium in this experiment.

All other characterization processes are presented in the Supplementary Materials.

3. Results

Figure 1a exhibits the evolutions of applied voltage with the oxidation period during MAO processes with and without the introduction of ultrasonic vibration (UV). Both curves exhibit a similar tendency, revealing that the cell voltage initially increases linearly, then increases at a slower rate, and finally stabilizes with slight fluctuation. Close examination reveals that, after the introduction of UV, the breakdown potential (~ 250 V) that reflects the initial dielectric breakdown of the coating is lower than that without the application of UV (~ 270 V). Similarly, the UV introduction also decreases the stabilized potential from ~ 490 V to ~ 475 V. In addition, the general appearances of the resultant coatings were recorded (Figure 1b,c), revealing that both coatings exhibit uniform brownish appearances regardless of UV introduction.

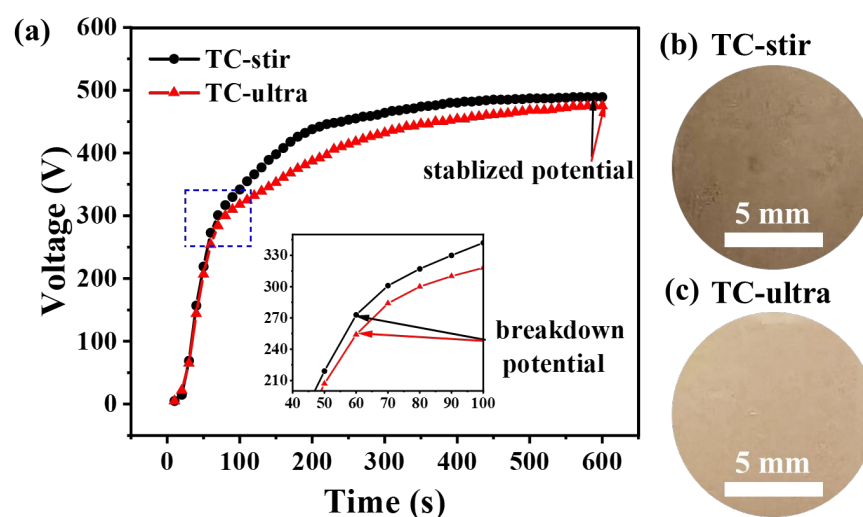


Figure 1. (a) Voltage–time curves during the micro-arc oxidation with and without the introduction of ultrasonic vibration; (b,c) surface appearances of both coatings.

After visual observation, the examination using a scanning electron microscope (SEM) was conducted for both coatings (Figure 2), revealing their similar appearances. Figure 2a,b display the general views of TC-stir and TC-ultra, exhibiting porous morphologies typical for micro-arc oxidized surfaces [49,50]. Framed areas in Figure 2a,b are magnified in Figure 2c,d. Micro-sized pores were observed in both coatings (denoted with white dashed line arrows). The area fractions of micro-sized pores were quantitatively analyzed to evaluate the porosities of both coatings. A minimum of 10 different surface views were analyzed (Figure S1), revealing that the porosity of TC-stir ($\sim 4.85\%$) is higher than that of TC-ultra ($\sim 4.03\%$). Moreover, the average pore size of TC-stir (~ 1.39 μm) remains similar to that of TC-ultra (~ 1.46 μm). Finally, the detailed morphological features are revealed in Figure 2e,f, corresponding to the framed areas in Figure 2c,d. Both nano-sized pores (denoted with dashed line arrows) and cracks (denoted with solid line arrows) were noticed in both coatings, which may originate from oxygen evolution and thermal stress during the oxidation process. Hence, from Figure 2, it is revealed that the UV introduction mainly reduces the porosity of the resultant ceramic coating.

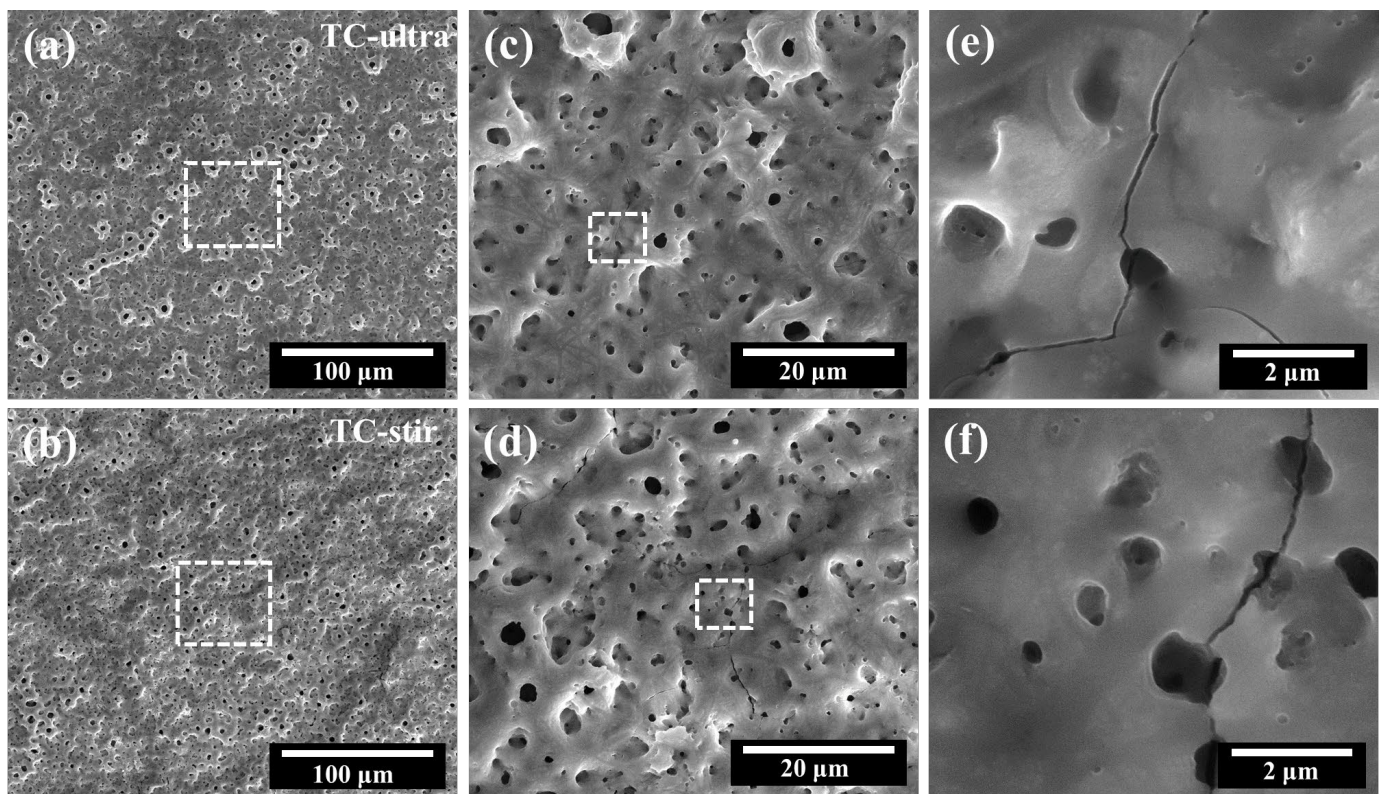


Figure 2. SEM micrographs of coating surfaces: (a,c,e) TC-ultra; (b,d,f) TC-stir.

An electron probe X-ray micro-analyzer (EPMA) was then conducted to examine the elemental profiles of both coatings. Figure 3a displays a typical area of TC-ultra along with the elemental distribution maps, which reveals that it contains Ti, Ca, P, and O as well as Cu. The successful incorporation of Cu into TiO_2 is revealed and the elemental distributions are relatively uniform. Similar to TC-ultra, Figure 3b reveals the uniform elemental distribution across TC-stir with the presence of Ti, Ca, P, O, and Cu. EDX point analysis was also conducted to quantify the chemical compositions for both coatings (Table 1). It is revealed that a relatively higher Cu content (~ 2.13 wt.%) is shown in TC-ultra relative to TC-stir (~ 1.39 wt.%), indicating that UV may enhance the incorporation of Cu into TiO_2 during the MAO process.

The cross-sectional views of both coatings are shown in Figure 4. Figure 4a exhibits a typical cross-section of TC-ultra, revealing its thickness ranging from ~ 13.5 μm to ~ 26.2 μm . Morphological features were further presented in Figure 4b, exhibiting its bi-layered structure. The inner layer, which is approximately hundreds of nanometers in thickness is relatively compact, whereas the outer layer is increasingly defective with the presence of cracks (denoted with a solid line arrow) and pores of nanometer and micrometer scales (denoted with dashed line arrows). Similarly, the cross-sectional view of the brown area in TC-stir is shown in Figure 4c, suggesting its reduced thickness (ranging from ~ 8.1 μm to ~ 12.8 μm) relative to TC-ultra (ranging from ~ 13.5 μm to ~ 26.2 μm). The detailed morphological features are shown in Figure 4d, which again reveals its bi-layered structure, similar to Figure 4b. Hence, the cross-sectional examination reveals that coating thickness increases dramatically with the introduction of UV.

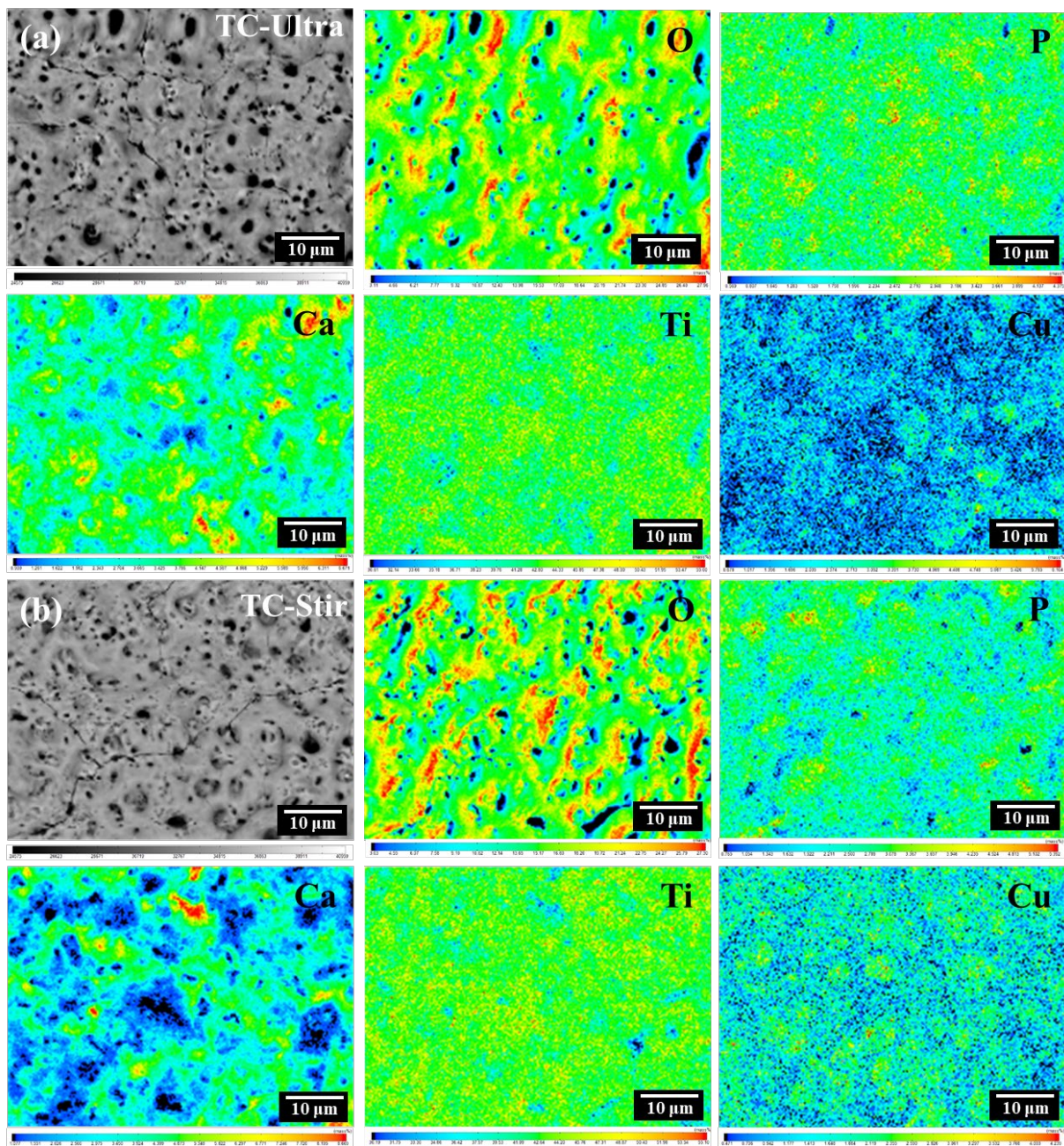


Figure 3. EPMA analysis of coating surfaces: (a) SEM micrograph of TC-ultra with the corresponding EDX maps in sequence of Ti, Cu, O, P, and Ca; (b) SEM micrograph of TC-stir with the corresponding EDX maps in sequence of Ti, Cu, O, P, and Ca.

Table 1. Quantitative analysis of both Cu-modified TiO₂ coatings.

Element	Contents (%)				
	Ti	O	Ca	P	Cu
TC-ultra	53.76	32.54	5.21	6.36	2.13
TC-stir	54.33	34.07	5.07	5.14	1.39

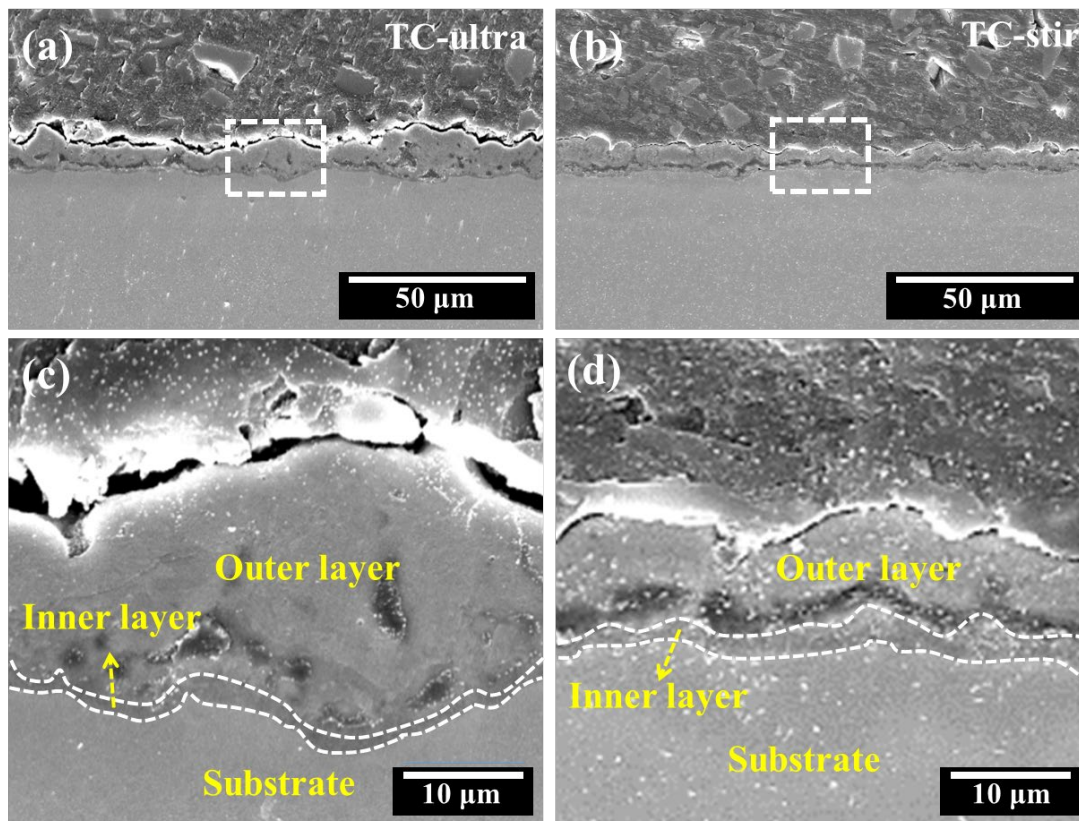


Figure 4. SEM micrographs of cross-sectional views in the coatings: (a,c) TC-ultra; (b,d) TC-stir.

Elemental profiles of the cross-sectional views were also examined by EPMA mapping analysis (Figure 5). Consistent with Figure 4, Cu, Ca, and P could be detected in both coatings, confirming their incorporation into TiO₂. Interestingly, their distributions are non-uniform with the penetration depths of P and Cu much larger than that of Ca. This may be associated with their different charged conditions since the external electric field may promote the migration of negatively charged species whereas the mass transfer for positively charged species may be hindered to a degree. As a result, both P and Cu existing as negatively charged species could penetrate deeper into the coating relative to Ca. Scrutiny of P and Cu maps also reveals their distinctive contents within the coatings. Since the incorporation of electrolytic components is closely associated with their mass transfer through the short-circuited pathways consisting of pores, cracks, and other defects in the ceramic coating, the reduced sizes of H_xPO₄^{(3-x)-} facilitate their mass transfer relative to larger Cu-EDTA complexes. In addition, it is also revealed that the Cu distribution is increasingly uniform in TC-ultra (Figure 5a) relative to TC-stir (Figure 5b), which may be attributed to the mechanical effect of UV as illustrated in the Section 4.

To investigate the influence of UV on phase components of the ceramic coating, thin film X-ray diffraction (TFXRD) analysis was carried out on both TC-ultra and TC-stir with the patterns shown in Figure 6. Peaks for anatase and rutile phases were observed in both XRD patterns. The proportions of anatase and rutile detected by the XRD were assessed by the following equation [13]:

$$W_R = 1 / (1 + 0.8I_A / I_R) \quad (1)$$

where I_A and I_R are the X-ray diffraction peak strengths of the anatase-phase (101) and rutile-phase (110) crystal planes, respectively. The corresponding results are shown in Figure 6b. Scrutiny of Figure 6 reveals that the anatase-to-rutile ratio of TC-ultra (~1.12) is lower than that of TC-stir (~1.44), which will be illustrated in the Section 4. Interestingly, no peaks corresponding to Cu-related components were detected.

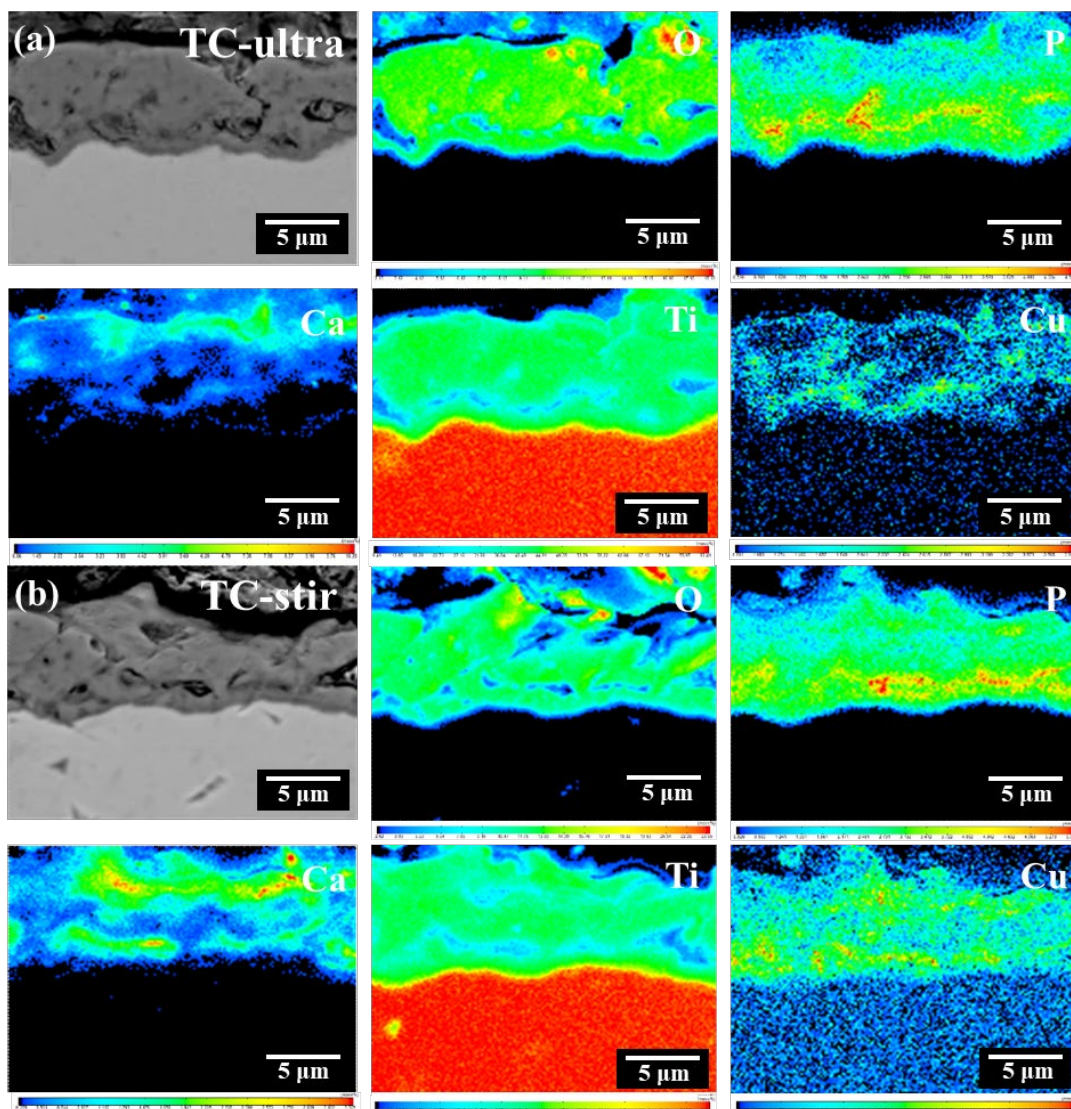


Figure 5. EPMA analysis of cross sections in both Cu-modified TiO₂ coatings: (a) TC-ultra, (b) TC-stir.

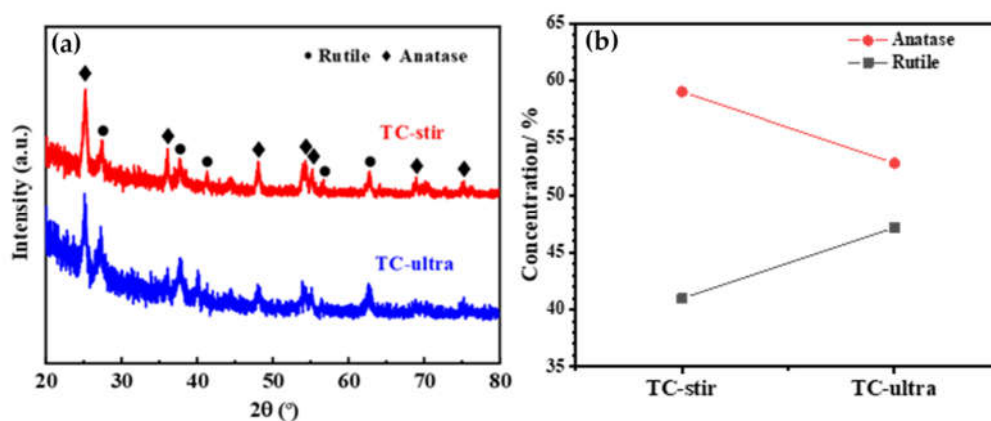


Figure 6. TFXRD patterns (a) and concentration (%) of rutile and anatase phases (b) of TC-stir and TC-ultra.

Further, to identify the surface elemental configuration of Cu species, X-ray photoelectron spectroscopy (XPS) analysis was conducted on both coatings (Figure 7). From the survey (Figure 7a), it is obvious that both coatings contain Ti, O, Ca, P, and Cu. High-

resolution XPS spectra for Cu 2p are shown in Figure 7b, and both contain four characteristic peaks located at 933.2 eV and 952.0 eV for Cu⁺ and 935.7 eV and 955.8 eV for Cu²⁺ and satellite peaks at 944.7 eV and 964.8 eV [33]. Hence, it is indicated that both Cu⁺ and Cu²⁺ were present. Scrutiny of Figure 7b reveals the significant difference in the Cu²⁺-to-Cu⁺ ratio. In TC-stir, the Cu²⁺-to-Cu⁺ ratio is only ~0.343, which is lower than that of TC-ultra (~0.423) (Figure 7b), which indicates that UV may promote the formation of Cu²⁺ in the Cu-modified TiO₂ coating.

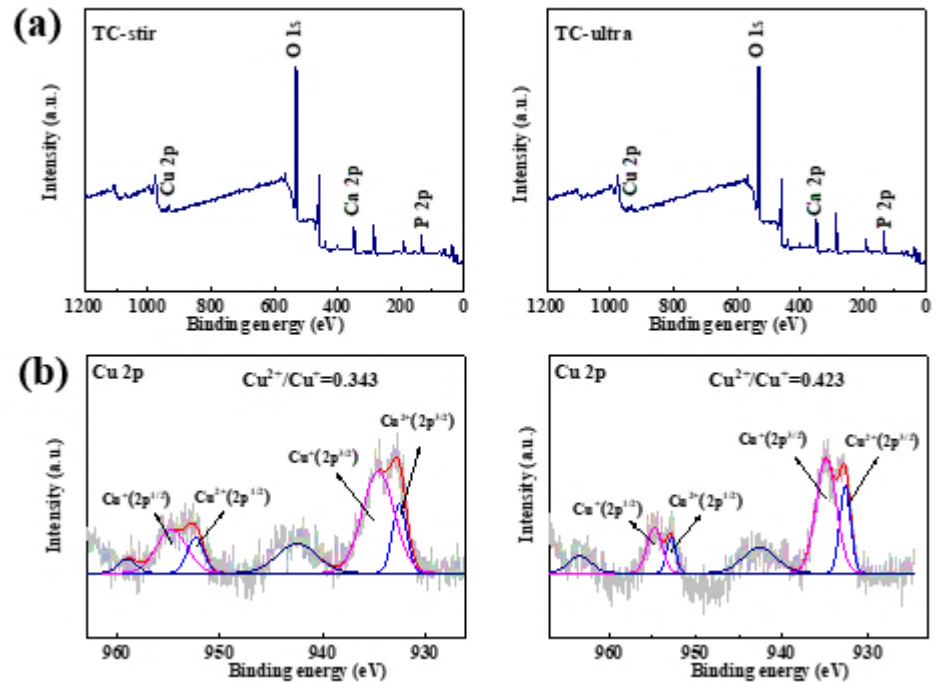


Figure 7. (a) XPS surveys; (b) high-resolution XPS spectra of Cu in both Cu-modified TiO₂ coatings.

Afterward, the surface conditions of both coatings were examined. Water contact angles (WCAs) of both coatings were examined (Figure 8a). TC-ultra and TC-stir exhibit WCAs of ~46.1° and ~47.3°, indicating their similar surface wettability. Further, their surface topographies are shown in Figure 8b. The surface roughness of TC-ultra is ~1.11 μm, which is similar to that of TC-stir (~1.05 μm). Hence, their surface conditions remain similar regardless of the application of UV or not.

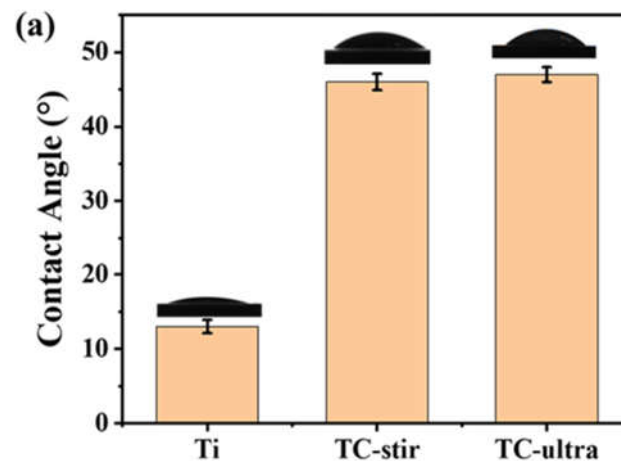


Figure 8. Cont.

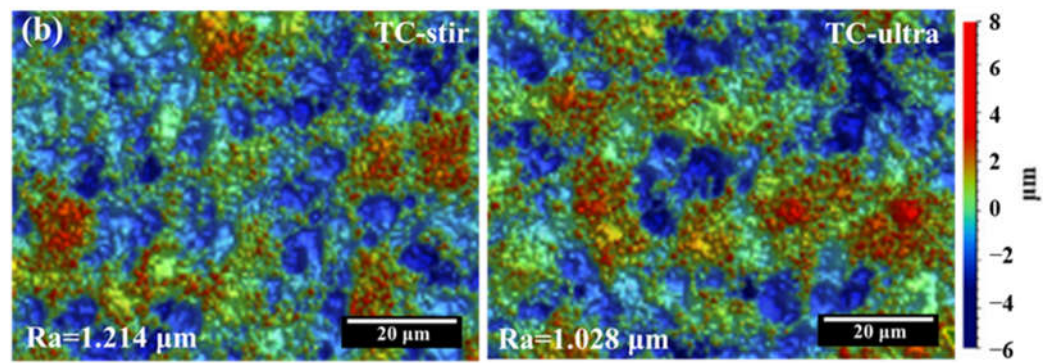


Figure 8. (a) Water contact angles and (b) surface topography for both Cu-modified TiO₂ coatings.

The electrochemical responses were recorded to assess the corrosion resistance of both coatings. For comparison, bare Ti was also examined. Figure 9a displays the potentiodynamic polarization (PDP) curves with the fitting results listed in Table 2. The corrosion potential (E_{corr}) follows the decreasing order: TC-ultra (~ -0.173 V) > TC-stir (~ -0.153 V) > Ti (~ -0.185 V) and the corrosion current density (i_{corr}) exhibits the decreasing order: Ti ($\sim 2.12 \times 10^{-7}$ A/cm²) > TC-stir ($\sim 5.21 \times 10^{-8}$ A/cm²) > TC-ultra ($\sim 1.37 \times 10^{-9}$ A/cm²). Thus, it is suggested that the corrosion resistance follows the decreasing order: TC-ultra > TC-stir > Ti.

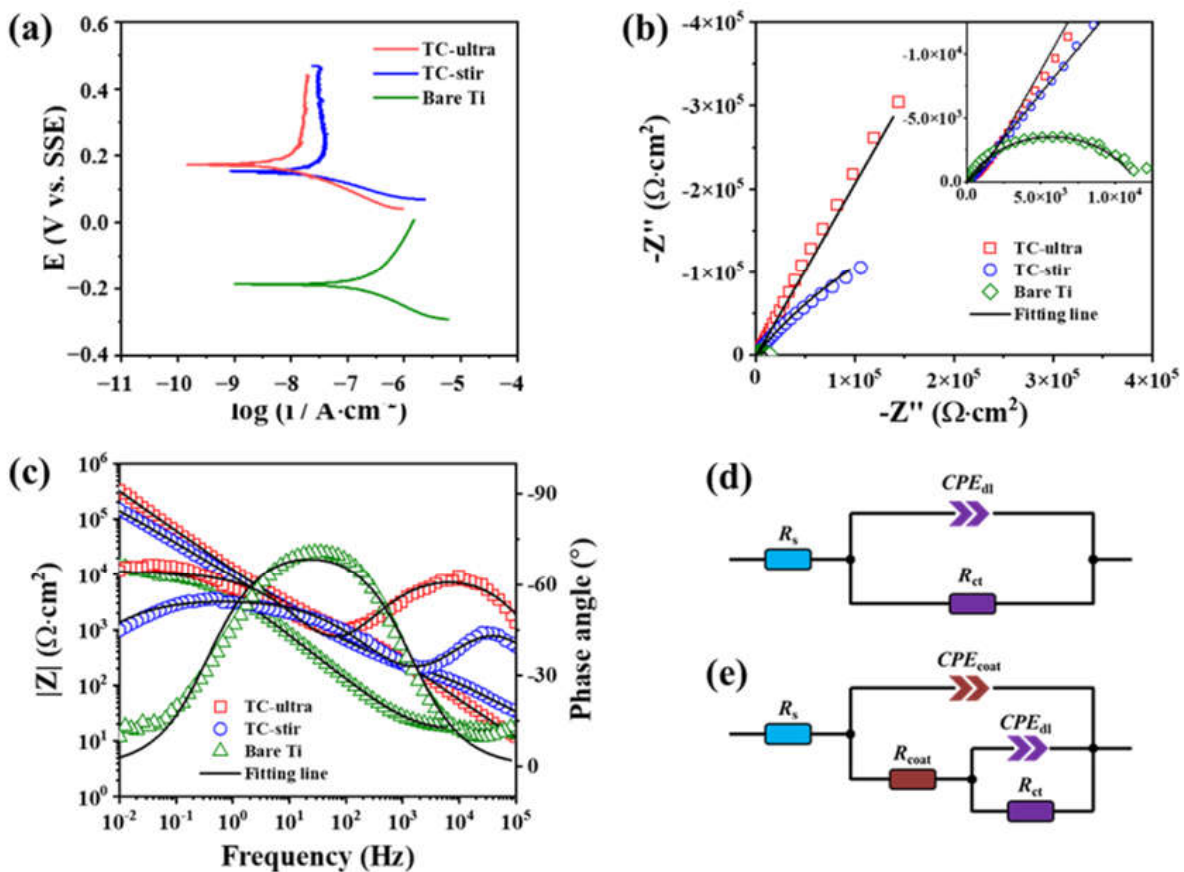


Figure 9. Electrochemical measurements for TC-stir and TC-ultra: (a) potentiodynamic polarization curves; (b) Nyquist plots of EIS; (c) Bode plots of EIS; and (d,e) equivalent circuit (EC) model for EIS.

Table 2. Tafel slopes (β_a and β_c), corrosion current densities (i_{corr}), and corrosion potentials (E_{corr}) derived from the potentiodynamic polarization curves in Figure 9a.

Samples	β_a (mV)	β_c (mV)	i_{corr} (A/cm ²)	E_{corr} (V)
TC-ultra	519.54	81.58	1.37×10^{-9}	0.173
TC-stir	601.94	40.33	5.21×10^{-8}	0.153
Bare Ti	286.27	115.12	2.12×10^{-7}	−0.185

Electrochemical impedance spectroscopy (EIS) analysis was also conducted with the Nyquist and Bode plots shown in Figure 9b,c. From the Nyquist plots (Figure 9c), two capacitive loops are revealed for both TC-ultra and TC-stir, which correspond to electrolyte/coating and electrolyte/substrate interfaces, respectively. By contrast, only one capacitive loop could be observed for bare Ti. According to the Bode plots (Figure 9d), the impedance modulus ($|Z|$) at 0.01 Hz, which represents corrosion resistance, follows a decreasing order: TC-ultra > TC-stir > Ti. Thus, it is indicated that enhanced corrosion resistance of TC-ultra was achieved relative to TC-stir.

Based on Figure 9b,c, the equivalent circuit (EC) models of Figure 9d,e were applied to explain EIS data. Considering the current dispersion effect, a constant phase angle element (CPE) was applied. A detailed description of the EC models has been reported previously [49]. The fitting results are listed in Table 3. The sum of R_{coat} and R_{ct} for all layers indicated that corrosion resistance follows a decreasing order: TC-ultra > TC-stir > Ti, again demonstrating that TC-ultra exhibits an enhanced corrosion resistance relative to TC-stir and bare Ti, confirming the beneficial role of UV on the anti-corrosion property of Cu-modified TiO₂ coatings.

Table 3. Fitting results of EIS data (Figure 9b,c) of both Cu-modified TiO₂ coatings.

Samples	R_s ($\Omega \cdot \text{cm}^2$)	CPE_{coat-Q} (F/cm ²)	CPE_{coat-n}	R_{coat} ($\Omega \cdot \text{cm}^2$)	CPE_{dl-Q} (F/cm ²)	CPE_{dl-n}	R_{ct} ($\Omega \cdot \text{cm}^2$)
TC-ultra	13.57	5.84×10^{-6}	0.728	1519	1.68×10^{-5}	0.710	2.68×10^5
TC-stir	16.33	1.19×10^{-6}	0.703	1822	2.12×10^{-5}	0.701	1.03×10^5
Bare Ti	15.12	/	/	/	4.45×10^{-5}	0.703	1.14×10^4

The antifouling capability of TC-stir and TC-ultra against SRB bacteria was assessed with Ti as a comparison. It has been well documented that bare Ti exhibits limited antifouling efficacy and is thus considered to be a negative control group.

After immersion in the SRB culture media for 14 days, SEM was employed to examine their surface features with representative results shown in Figure 10. The general view of bare Ti (Figure 10a) shows a high number of bright features whereas both coatings maintain porous features (Figure 10b,c), similar to their original morphology. Figure 10d–f correspond to the framed areas of Figure 10a–c at increased magnifications. As shown in Figure 10d, in addition to micron-sized SRB with rod shapes, flocculent features, supposed to be the extracellular polymeric substance (EPS) produced by SRB, could also be noticed in the periphery, which may contribute to the formation of a bio-film. Further scrutiny of Figure 10e,f also indicates the presence of a relatively higher amount of SRB on TC-stir relative to TC-ultra, preliminarily indicating the enhanced antifouling capability of Cu-modified TiO₂ coatings produced via UV assistance. Finally, the detailed morphology of bacteria is shown in Figure 10g–i. Clearly, a bio-film consisting of SRB and EPS has been formed on bare Ti (Figure 10g). For TC-stir, pumped and lysed bacteria co-exist with the presence of metabolism producing live SRB in the periphery (Figure 10g), whereas only SRBs with damaged membranes were observed on the surface of TC-ultra (Figure 10i), confirming the enhanced antifouling capability of TC-ultra relative to TC-stir after 14 days incubation.

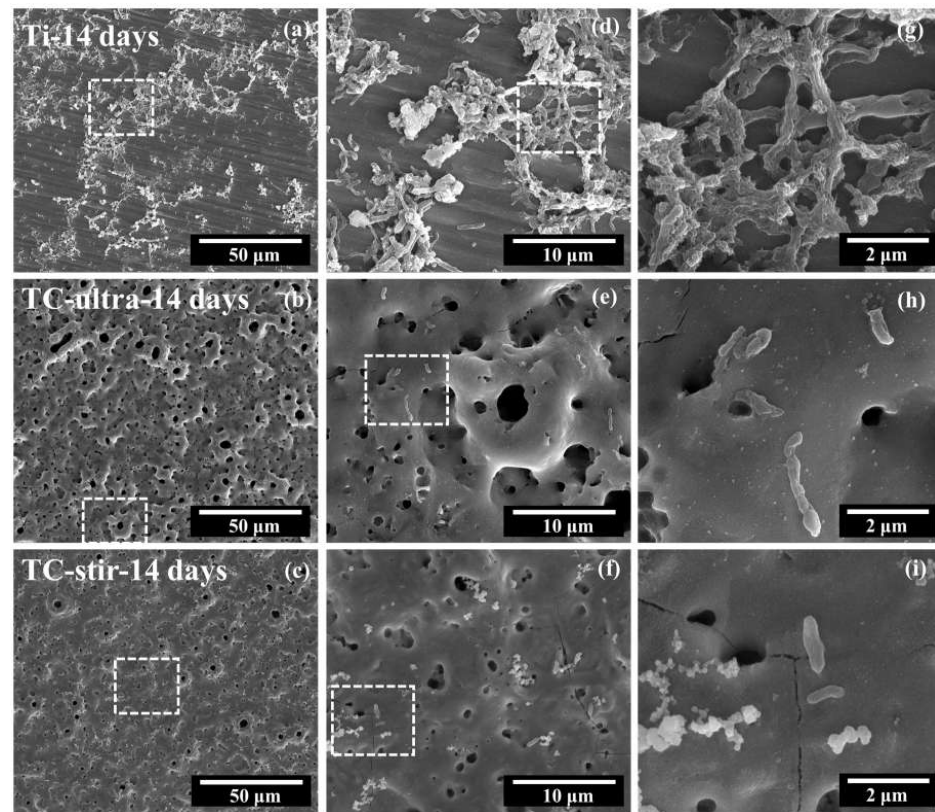
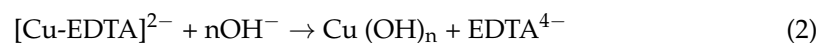


Figure 10. SEM micrographs of SRB on the surfaces of both Cu-modified TiO₂ coatings with metallic Ti as a comparison after immersion for 14 days: (a,d,g) Ti, (b,e,h) TC-ultra and (c,f,i) TC-stir.

4. Discussion

Comparing the microstructural features and coating properties between TC-stir and TC-ultra, it is revealed that UV introduction dramatically affects the microstructure (Figures 1–8), corrosion resistance (Figure 9), and antifouling capability against SRB (Figure 10) of Cu-modified TiO₂ coatings, which may be ascribed to the unique characteristics of ultrasonic waves. During the MAO process, Cu could be incorporated into TiO₂ via the following reactions [34,51]:



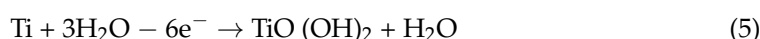
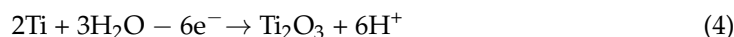
As reported previously, UV may cause defects in solids due to its related stress [25,52], which promotes the micro-arc discharges and thus contributes to the growth of ceramic oxide by healing the defects [50]. Hence, the introduction of UV induces defects and increases the population density of micro-arc discharges to promote Reactions (1) and (2) for Cu incorporation. In addition, the mechanical mixing effect of UV may also promote the migration of Cu-EDTA complexes to benefit Cu incorporation into TiO₂ [25,52]. Hence, the introduction of UV is conducive to the incorporation of Cu into TiO₂, which results in a higher content of Cu in TC-ultra relative to TC-stir (Table 1). Similarly, the enhanced micro-arc discharges associated with UV promote the formation of molten oxide, which results in the reduction in defectiveness (Figure S1) and the increase in coating thickness (Figure 4) of TC-ultra relative to TC-stir.

In addition, the difference in phase components is related to UV introduction. The rapid cooling rate induced by electrolytes hinders the transformation of the metastable phase to the thermodynamically favored phase. As a result, the metastable anatase TiO₂ phase exists in both coatings, which may transform into the thermodynamically favored rutile phase when a proper condition is provided. The mechanical effect of UV increases the kinetic energy of oxygen atoms, which promotes atomic diffusion and thus the transformation

from anatase to rutile. Hence, a reduced anatase-to-rutile ratio is achieved in TC-ultra relative to TC-stir (Figure 6).

Finally, the chemical condition of Cu in TiO₂ is also affected by the introduction of UV. As mentioned above, the defects induced by UV facilitate the breakdown of oxide, which lowers its breakdown potential and also results in a lower released energy density at the micro-arc discharge site [8,11]. Hence, a lower average temperature is expected, which favors the formation of Cu²⁺ rather than Cu⁺ [34]. Hence, relative to TC-stir, a reduced Cu⁺-to-Cu²⁺ ratio was achieved in TC-ultra (Figure 7).

The electrochemical corrosion of titanium in NaCl solution usually involves the following reactions [53,54]:



The barrier of the oxide ceramic layer on the Ti/MAO surface weakened the erosion of the aggressive ion Cl⁻ compared to pure Cu. The difference in microstructural features results in their different corrosion resistance (Figure 9). Generally, the corrosion resistance of a ceramic oxide is closely related to its capability to inhibit electrolytic penetration to the coating/substrate interface. Thus, the thickness, defectiveness, and hydrophobicity are crucial to its capability to act as a physical barrier to hinder electrolytic penetration [28]. As a result, the difference in coating thickness (Figure 4) and defectiveness (Figures 2 and S1) determines their different corrosion resistance, especially considering their similar surface conditions (Figure 8). Since TC-ultra possesses enhanced thickness and reduced defectiveness relative to TC-stir, the improved corrosion resistance of TC-ultra compared to TC-stir is expected as confirmed in Figure 9.

Generally, the antifouling capability is closely associated with surface chemistry and surface topography [11,16,36,55,56], which may affect the adhesion and proliferation of microorganisms. Considering the similar surface conditions of both Cu-modified TiO₂ coatings (Figure 8), it is indicated that surface chemistry plays a more crucial role in antifouling capability, which may be ascribed to Cu incorporation associated with UV introduction as mentioned above (Figure 3 and Table 1).

After the adhesion of SRB, the surface chemistry may interrupt their proliferation due to the high antibacterial efficiency of Cu species, which results in a higher antifouling capability of Cu-modified TiO₂ coating relative to bare Ti (Figure 10). Due to the low released Cu dosage relative to its minimum inhibitory concentration (MIC) [11,44,45,57], it is then believed that the Cu²⁺ and Cu⁺ within TiO₂ act as effective agents to hinder the proliferation of SRB. It has been well documented that the antibacterial capability of Cu²⁺ is attributed to the reactive oxygen species that damage cell membranes [44]. Unlike Cu²⁺, Cu⁺ has an enhanced affinity towards proteins and thus disables the replica capability of bacteria [38,58–60]. Since both Cu²⁺ and Cu⁺ contribute to the bactericidal effect of SRB and thereby effectively inhibit their growth, it is expected that the higher Cu content in TC-ultra results in its higher antifouling capability relative to TC-stir (Figure 10).

5. Conclusions

In the present work, the influence of ultrasonic vibration on the microstructure, corrosion resistance, and antifouling properties of Cu-modified TiO₂ coatings produced by MAO was systematically studied. It is revealed that the introduction of ultrasonic vibration optimizes the microstructural features, corrosion resistance, and antifouling capability of Cu-modified TiO₂ coating, which enhances the surface performance of metallic Ti to fit marine engineering.

- With the introduction of UV, an increased content of Cu could be incorporated into TiO₂, which exhibits a higher Cu²⁺-to-Cu⁺ ratio relative to that without UV. The introduction of UV also promotes the growth of ceramic coating and affects the phase components of the coating with a higher rutile-to-anatase ratio achieved.
- Enhanced corrosion resistance of the Cu-modified TiO₂ coating could be achieved with the introduction of UV.
- UV introduction enhances Cu incorporation to benefit the antifouling capability of Cu-modified TiO₂ coatings.

Supplementary Materials: The following supporting information can be downloaded at: <https://www.mdpi.com/article/10.3390/coatings14040376/s1>, Figure S1. Porosity analysis of both Cu-modified TiO₂ coatings.

Author Contributions: Conceptualization, G.C.; methodology, P.H., L.Z. and G.C.; software, P.H. and L.Z.; validation, Y.L. and X.Z.; formal analysis, P.H. and G.C.; investigation, P.H., L.Z. and G.C.; data curation, Y.L. and J.L.; writing—original draft preparation, P.H. and L.Z.; writing—review and editing, G.C.; supervision, Y.L. and X.Z.; funding acquisition, G.C. and X.Z. All authors have read and agreed to the published version of the manuscript.

Funding: The authors thank the financial support from National Natural Science Foundation of China (No. 52371065) and Hubei Provincial Natural Science Foundation of China (No. 2023AFB637).

Institutional Review Board Statement: Not applicable.

Informed Consent Statement: Not applicable.

Data Availability Statement: Data are contained within the article and Supplementary Materials.

Acknowledgments: The authors also thank the technical support from the Analytical and Testing Centre at Huazhong University of Science and Technology, the Instrumental Analysis and Research Centre of Shanghai Yanku (www.shuyanku.com, accessed on 18 November 2022), Shiyanjia Lab (www.shiyanjia.com, accessed on 25 November 2022), Experiment Centre for Advanced Manufacturing and Technology in School of Mechanical Science and Engineering of HUST and Nanoscale Characterization and Devices (CNCD). All research data supporting this publication are directly available within this publication.

Conflicts of Interest: Author Jiejun Liu was employed by the company Xiangtan Electric Power Co., Ltd. The remaining authors declare that the research was conducted in the absence of any commercial or financial relationships that could be construed as a potential conflict of interest.

References

1. Gorynin, I.V. Titanium alloys for marine application. *Mater. Sci. Eng. A* **1999**, *263*, 112–116. [[CrossRef](#)]
2. Wake, H.; Takahashi, H.; Takimoto, T.; Takayanagi, H.; Ozawa, K.; Kadoi, H.; Okochi, M.; Matsunaga, T. Development of an electrochemical antifouling system for seawater cooling pipelines of power plants using titanium. *Biotechnol. Bioeng.* **2006**, *95*, 468–473. [[CrossRef](#)]
3. Gusmano, G.; Montesperelli, G.; Forte, G.; Olzi, E.; Benedetti, A. On-line corrosion resistance tests in sea water on metals for MED plants. *Desalination* **2005**, *183*, 187–194. [[CrossRef](#)]
4. Been, J.; Faller, K. Using Ti-5111 for marine fastener applications. *JOM* **1999**, *51*, 21–24. [[CrossRef](#)]
5. Oryshchenko, A.S.; Gorynin, I.V.; Leonov, V.P.; Kudryavtsev, A.S.; Mikhailov, V.I.; Chudakov, E.V. Marine titanium alloys: Present and future. *Inorg. Mater. Appl. Res.* **2015**, *6*, 571–579. [[CrossRef](#)]
6. Yan, S.; Song, G.-L.; Li, Z.; Wang, H.; Zheng, D.; Cao, F.; Horynova, M.; Dargusch, M.S.; Zhou, L. A state-of-the-art review on passivation and biofouling of Ti and its alloys in marine environments. *J. Mater. Sci. Technol.* **2018**, *34*, 421–435. [[CrossRef](#)]
7. Zhang, X.; Yu, Y.; Jiang, D.; Jiao, Y.; Wu, Y.; Peng, Z.; Zhou, J.; Wu, J.; Dong, Z. Synthesis and characterization of a bi-functional hydroxyapatite/Cu-doped TiO₂ composite coating. *Ceram. Int.* **2019**, *45*, 6693–6701. [[CrossRef](#)]
8. Zhang, X.; Li, C.; Yu, Y.; Lu, X.; Lv, Y.; Jiang, D.; Peng, Z.; Zhou, J.; Zhang, X.; Sun, S.; et al. Characterization and property of bifunctional Zn-incorporated TiO₂ micro-arc oxidation coatings: The influence of different Zn sources. *Ceram. Int.* **2019**, *45*, 19747–19756. [[CrossRef](#)]
9. Zhang, C.; Wen, F.; Cao, Y. Progress in Research of Corrosion and Protection by Sulfate-Reducing Bacteria. *Procedia Environ. Sci.* **2011**, *10*, 1177–1182. [[CrossRef](#)]
10. Rao, T.S.; Kora, A.J.; Anupkumar, B.; Narasimhan, S.V.; Feser, R. Pitting corrosion of titanium by a freshwater strain of sulphate reducing bacteria (*Desulfovibrio vulgaris*). *Corros. Sci.* **2005**, *47*, 1071–1084. [[CrossRef](#)]

11. Zhang, X.; Wu, Y.; Wang, J.; Xia, X.; Lv, Y.; Cai, G.; Liu, H.; Xiao, J.; Liu, B.; Dong, Z. Microstructure, formation mechanism and antifouling property of multi-layered Cu-incorporated Al₂O₃ coating fabricated through plasma electrolytic oxidation. *Ceram. Int.* **2019**, *46*, 2901–2909. [[CrossRef](#)]
12. Kumar, S.; Roy, D.N.; Dey, V. A comprehensive review on techniques to create the anti-microbial surface of biomaterials to intervene in biofouling. *Colloid Interface Sci. Commun.* **2021**, *43*, 100464. [[CrossRef](#)]
13. Yao, J.; Wang, Y.; Wu, G.; Sun, M.; Wang, M.; Zhang, Q. Growth characteristics and properties of micro-arc oxidation coating on SLM-produced TC4 alloy for biomedical applications. *Appl. Surf. Sci.* **2019**, *479*, 727–737. [[CrossRef](#)]
14. Qian, P.Y.; Xu, Y.; Fusetani, N. Natural products as antifouling compounds: Recent progress and future perspectives. *Biofouling* **2010**, *26*, 223–234. [[CrossRef](#)]
15. Tian, J.J.; Xu, K.W.; Hu, J.H.; Zhang, S.J.; Cao, G.Q.; Shao, G.S. Durable self-polishing antifouling Cu-Ti coating by a micron-scale Cu/Ti laminated microstructure design. *J. Mater. Sci. Technol.* **2021**, *79*, 62–74. [[CrossRef](#)]
16. Liu, M.Y.; Li, S.N.; Wang, H.; Jiang, R.J.; Zhou, X. Research progress of environmentally friendly marine antifouling coatings. *Polym. Chem.* **2021**, *12*, 3702–3720. [[CrossRef](#)]
17. Lazorenko, G.; Kasprzhitskii, A.; Nazdracheva, T. Anti-corrosion coatings for protection of steel railway structures exposed to atmospheric environments: A review. *Constr. Build. Mater.* **2021**, *288*, 123115. [[CrossRef](#)]
18. Chouirfa, H.; Bouloussa, H.; Migonney, V.; Falentin-Daudré, C. Review of titanium surface modification techniques and coatings for antibacterial applications. *Acta Biomater.* **2019**, *83*, 37–54. [[CrossRef](#)]
19. Zambrano, D.F.; Barrios, A.; Tobón, L.E.; Serna, C.; Gómez, P.; Osorio, J.D.; Toro, A. Thermal properties and phase stability of Yttria-Stabilized Zirconia (YSZ) coating deposited by Air Plasma Spray onto a Ni-base superalloy. *Ceram. Int.* **2018**, *44*, 3625–3635. [[CrossRef](#)]
20. Schwartz, A.; Kossenko, A.; Zinigrad, M.; Danchuk, V.; Sobolev, A. Cleaning Strategies of Synthesized Bioactive Coatings by PEO on Ti-6Al-4V Alloys of Organic Contaminations. *Materials* **2023**, *16*, 4624. [[CrossRef](#)]
21. Santecchia, E.; Hamouda, A.M.S.; Musharavati, F.; Zalnezhad, E.; Cabibbo, M.; Spigarelli, S. Wear resistance investigation of titanium nitride-based coatings. *Ceram. Int.* **2015**, *41*, 10349–10379. [[CrossRef](#)]
22. Zhou, P.; Yang, L.; Hou, Y.; Duan, G.; Yu, B.; Li, X.; Zhai, Y.; Zhang, B.; Zhang, T.; Wang, F. Grain refinement promotes the formation of phosphate conversion coating on Mg alloy AZ91D with high corrosion resistance and low electrical contact resistance. *Corros. Commun.* **2021**, *1*, 47–57. [[CrossRef](#)]
23. Yang, L.; Zhou, X.R.; Curioni, M.; Pawar, S.; Liu, H.; Fan, Z.Y.; Scamans, G.; Thompson, G. Corrosion Behavior of Pure Magnesium with Low Iron Content in 3.5 wt% NaCl Solution. *J. Electrochem. Soc.* **2015**, *162*, C362–C368. [[CrossRef](#)]
24. Zhu, L.; Guo, Z.; Zhang, Y.; Li, Z.; Sui, M. A mechanism for the growth of a plasma electrolytic oxide coating on Al. *Electrochim. Acta* **2016**, *208*, 296–303. [[CrossRef](#)]
25. He, D.; Li, G.; Shen, D.; Guo, C.; Ma, H.; Cai, J. Effect mechanism of ultrasound on growth of micro-arc oxidation coatings on A96061 aluminum alloy. *Vacuum* **2014**, *107*, 99–102. [[CrossRef](#)]
26. Shao, Y.; Zeng, R.-C.; Li, S.-Q.; Cui, L.-Y.; Zou, Y.-H.; Guan, S.-K.; Zheng, Y.-F. Advance in Antibacterial Magnesium Alloys and Surface Coatings on Magnesium Alloys: A Review. *Acta Metall. Sin. (Engl. Lett.)* **2020**, *33*, 615–629. [[CrossRef](#)]
27. Nahum, E.Z.; Lugovskoy, S.; Lugovskoy, A.; Kazanski, B.; Sobolev, A. The study of hydroxyapatite growth kinetics on CP—Ti and Ti65Zr treated by Plasma electrolytic oxidation process. *J. Mater. Res. Technol.* **2023**, *24*, 2169–2186. [[CrossRef](#)]
28. Buchheit, R.G. A Compilation of Corrosion Potentials Reported for Intermetallic Phases in Aluminum Alloys. *J. Electrochem. Soc.* **1995**, *142*, 3994–3996. [[CrossRef](#)]
29. Guo, H.; Liu, Z.; Wang, Y.; Li, J. Tribological mechanism of micro-arc oxidation coatings prepared by different electrolyte systems in artificial seawater. *Ceram. Int.* **2021**, *47*, 7344–7352. [[CrossRef](#)]
30. Dou, W.W.; Pu, Y.N.; Han, X.M.; Song, Y.; Chen, S.G.; Gu, T.Y. Corrosion of Cu by a sulfate reducing bacterium in anaerobic vials with different headspace volumes. *Bioelectrochemistry* **2020**, *133*, 107478. [[CrossRef](#)] [[PubMed](#)]
31. Javed, M.A.; Neil, W.C.; McAdam, G.; Wade, S.A. Effect of sulphate-reducing bacteria on the microbiologically influenced corrosion of ten different metals using constant test conditions. *Int. Biodeterior. Biodegrad.* **2017**, *125*, 73–85. [[CrossRef](#)]
32. Cui, M.; Jo, Y.H.; Kayani, S.H.; Kim, H.-W.; Lee, J.-H. Effects of Cu additions on the precipitation activation energy and mechanical properties of prestrained Al-Mg-Si alloys. *J. Mater. Res. Technol.* **2022**, *20*, 2629–2637. [[CrossRef](#)]
33. Li, H.; Yan, Z.; Cao, L. Bake hardening behavior and precipitation kinetic of a novel Al-Mg-Si-Cu aluminum alloy for lightweight automotive body. *Mater. Sci. Eng. A* **2018**, *728*, 88–94. [[CrossRef](#)]
34. Zhang, X.; Peng, Z.; Lu, X.; Lv, Y.; Cai, G.; Yang, L.; Dong, Z. Microstructural evolution and biological performance of Cu-incorporated TiO₂ coating fabricated through one-step micro-arc oxidation. *Appl. Surf. Sci.* **2019**, *508*, 144766. [[CrossRef](#)]
35. Qi, Y.; Liang, W.; Miao, Q.; Lin, H.; An, H.; Liu, Y.; Zuo, S.; Ma, H. Corrosion behavior and antifouling ability of Cu-Zn-Al/Zn-Al composite coating on Q235 steel. *Surf. Coat. Technol.* **2021**, *405*, 126614. [[CrossRef](#)]
36. Cerchier, P.; Pezzato, L.; Moschin, E.; Coelho, L.B.; Olivier, M.G.M.; Moro, I.; Magrini, M. Antifouling properties of different Plasma Electrolytic Oxidation coatings on 7075 aluminium alloy. *Int. Biodeterior. Biodegrad.* **2018**, *133*, 70–78. [[CrossRef](#)]
37. Chen, J.; Zhang, Y.; Ibrahim, M.; Etim, I.P.; Tan, L.; Yang, K. In vitro degradation and antibacterial property of a copper-containing micro-arc oxidation coating on Mg-2Zn-1Gd-0.5Zr alloy. *Colloids Surf. B Biointerfaces* **2019**, *179*, 77–86. [[CrossRef](#)]
38. Liu, R.; Memarzadeh, K.; Chang, B.; Zhang, Y.; Ma, Z.; Allaker, R.P.; Ren, L.; Yang, K. Antibacterial effect of copper-bearing titanium alloy (Ti-Cu) against *Streptococcus mutans* and *Porphyromonas gingivalis*. *Sci. Rep.* **2016**, *6*, 29985. [[CrossRef](#)]

39. Wu, H.; Zhang, X.; Geng, Z.; Yin, Y.; Hang, R.; Huang, X.; Yao, X.; Tang, B. Preparation, antibacterial effects and corrosion resistant of porous Cu–TiO₂ coatings. *Appl. Surf. Sci.* **2014**, *308*, 43–49. [[CrossRef](#)]
40. Stranak, V.; Wulff, H.; Rebl, H.; Zietz, C.; Arndt, K.; Bogdanowicz, R.; Nebe, B.; Bader, R.; Podbielski, A.; Hubicka, Z.; et al. Deposition of thin titanium–copper films with antimicrobial effect by advanced magnetron sputtering methods. *Mater. Sci. Eng. C* **2011**, *31*, 1512–1519. [[CrossRef](#)]
41. Zhu, W.; Zhang, Z.; Gu, B.; Sun, J.; Zhu, L. Biological Activity and Antibacterial Property of Nano-structured TiO₂ Coating Incorporated with Cu Prepared by Micro-arc Oxidation. *J. Mater. Sci. Technol.* **2013**, *29*, 237–244. [[CrossRef](#)]
42. Rokosz, K.; Hryniewicz, T.; Matysek, D.; Raaen, S.; Valicek, J.; Dudek, L.; Harnicarova, M. SEM, EDS and XPS Analysis of the Coatings Obtained on Titanium after Plasma Electrolytic Oxidation in Electrolytes Containing Copper Nitrate. *Materials* **2016**, *9*, 318. [[CrossRef](#)] [[PubMed](#)]
43. Zhang, X.; Li, J.; Wang, X.; Wang, Y.; Hang, R.; Huang, X.; Tang, B.; Chu, P.K. Effects of copper nanoparticles in porous TiO₂ coatings on bacterial resistance and cytocompatibility of osteoblasts and endothelial cells. *Mater. Sci. Eng. C* **2018**, *82*, 110–120. [[CrossRef](#)] [[PubMed](#)]
44. Zhang, X.; Zhang, T.; Lv, Y.; Zhang, Y.; Lu, X.; Xiao, J.; Ma, C.; Li, Z.; Dong, Z. Enhanced uniformity, corrosion resistance and biological performance of Cu-incorporated TiO₂ coating produced by ultrasound-auxiliary micro-arc oxidation. *Appl. Surf. Sci.* **2021**, *569*, 150932. [[CrossRef](#)]
45. Zhang, E.; Zhao, X.; Hu, J.; Wang, R.; Fu, S.; Qin, G. Antibacterial metals and alloys for potential biomedical implants. *Bioact. Mater.* **2021**, *6*, 2569–2612. [[CrossRef](#)] [[PubMed](#)]
46. Wang, J.-L.; Xu, J.-K.; Hopkins, C.; Chow, D.H.-K.; Qin, L. Biodegradable Magnesium-Based Implants in Orthopedics—A General Review and Perspectives. *Adv. Sci.* **2020**, *7*, 1902443. [[CrossRef](#)]
47. Zhao, D.; Witte, F.; Lu, F.; Wang, J.; Li, J.; Qin, L. Current status on clinical applications of magnesium-based orthopaedic implants: A review from clinical translational perspective. *Biomaterials* **2017**, *112*, 287–302. [[CrossRef](#)]
48. Ribeiro, M.; Monteiro, F.J.; Ferraz, M.P. Infection of orthopedic implants with emphasis on bacterial adhesion process and techniques used in studying bacterial-material interactions. *Biomatter* **2012**, *2*, 176–194. [[CrossRef](#)]
49. Zhang, X.; Zhang, Y.; Lv, Y.; Dong, Z.; Yang, L.; Zhang, E.; Hashimoto, T.; Zhou, X. PEO coating on Mg–Ag alloy: The incorporation and release of Ag species. *J. Magnes. Alloys* **2022**, *11*, 2182–2195. [[CrossRef](#)]
50. Lv, Y.; Zhang, C.; Zhang, Y.; Wang, Q.; Zhang, X.; Dong, Z. Microstructure and Corrosion Resistance of Plasma Electrolytic Oxidized Recycled Mg Alloy. *Acta Metall. Sin. (Engl. Lett.)* **2022**, *35*, 961–974. [[CrossRef](#)]
51. Kamil, M.P.; Kaseem, M.; Ko, Y.G. Soft plasma electrolysis with complex ions for optimizing electrochemical performance. *Sci. Rep.* **2017**, *7*, 44458. [[CrossRef](#)]
52. Dejiu, S.; Jingrui, C.; Guolong, L.; Donglei, H.; Lailei, W.; Haojie, M.; Yonghong, X.; He, C.; Yaqian, Y. Effect of ultrasonic on microstructure and growth characteristics of micro-arc oxidation ceramic coatings on 6061 aluminum alloy. *Vacuum* **2014**, *99*, 143–148. [[CrossRef](#)]
53. Metikoš-Huković, M.; Kwokal, A.; Piljac, J. The influence of niobium and vanadium on passivity of titanium-based implants in physiological solution. *Biomaterials* **2003**, *24*, 3765–3775. [[CrossRef](#)] [[PubMed](#)]
54. Lu, W.Q.; Liu, Y.J.; Wu, X.; Liu, X.C.; Wang, J.C. Corrosion and passivation behavior of Ti-6Al-4V surfaces treated with high-energy pulsed laser: A comparative study of cast and 3D-printed specimens in a NaCl solution. *Surf. Coat. Technol.* **2023**, *470*, 129849. [[CrossRef](#)]
55. Gao, Z.; Jiang, S.; Zhang, Q.; Li, X. Advances in research of marine antifouling fluorine resin coatings with low surface energy. *Electroplat. Finish.* **2017**, *36*, 273–279.
56. Wang, J.; Yang, C.; Liu, S.; Fang, S.; Xia, C. Novel Antifouling Technology Research: Progress and Prospects. *Sci. Sin. Vitae* **2016**, *46*, 1079–1084.
57. Utgikar, V.P.; Tabak, H.H.; Haines, J.R.; Govind, R. Quantification of toxic and inhibitory impact of copper and zinc on mixed cultures of sulfate-reducing bacteria. *Biotechnol. Bioeng.* **2003**, *82*, 306–312. [[CrossRef](#)] [[PubMed](#)]
58. Tweddle, D.; Johnson, J.A.; Kapoor, M.; Bikmukhametov, I.; Mileski, S.; Carsley, J.E.; Thompson, G.B. Atomic-scale Clustering in a High-strength Al–Mg–Si–Cu Alloy. *Materialia* **2022**, *26*, 101567. [[CrossRef](#)]
59. Zhou, X.; Thompson, G.E.; Habazaki, H.; Shimizu, K.; Skeldon, P.; Wood, G.C. Copper enrichment in Al–Cu alloys due to electropolishing and anodic oxidation. *Thin Solid Film.* **1997**, *293*, 327–332. [[CrossRef](#)]
60. Qin, J.; Shi, X.T.; Li, H.Y.; Zhao, R.F.; Li, G.Q.; Zhang, S.F.; Ding, L.Y.; Cui, X.J.; Zhao, Y.; Zhang, R.F. Performance and failure process of green recycling solutions for preparing high degradation resistance coating on biomedical magnesium alloys. *Green Chem.* **2022**, *24*, 8113–8130. [[CrossRef](#)]

Disclaimer/Publisher’s Note: The statements, opinions and data contained in all publications are solely those of the individual author(s) and contributor(s) and not of MDPI and/or the editor(s). MDPI and/or the editor(s) disclaim responsibility for any injury to people or property resulting from any ideas, methods, instructions or products referred to in the content.